

Part 1
How Lipids Shape Proteins

1

Lipid Bilayers, Translocons and the Shaping of Polypeptide Structure

Stephen H. White, Tara Hessa, and Gunnar von Heijne

1.1 Introduction

Constitutive membrane proteins (MPs) come to equilibrium with the lipid bilayer and water, after transmembrane (TM) insertion, through the translocation machinery of cells. The prediction of their three-dimensional structure from the amino acid sequence should emerge from a comprehensive understanding of the physical chemistry of protein–lipid interactions. The most fundamental physical principle is that TM helices are composed predominantly of non-polar amino acids. Bacteriorhodopsin [1], comprised of seven TM helices packed neatly into a bundle, is generally taken as the archetypal MP. Its apparent simplicity has led to a simple prediction paradigm that involves first identifying hydrophobic TM segments using hydropathy plots (reviewed in [2]) and then applying helix-packing constraints [3]. This optimistic assessment has been seriously challenged by the three-dimensional structure of the ClC chloride channel published in 2002 [4] (Fig. 1.1A). The jumble of helices buried within the membrane mocks bacteriorhodopsin's simplicity. Not only do the 17-odd helices vary greatly in length and tilt, some form TM structures in end-to-end arrangements in the manner of the aquaporin family of transporters (reviewed in [5]). Hydropathy plots fail to identify the complex topology correctly. This failure is not limited to the ClC channel alone, as shown by the three-dimensional structure of the KvAP voltage-gated potassium channel [6]. The S1–S4 voltage sensing region is not comprised of the simple TM helices as surmised from hydropathy plot analyses. Rather, this region appears to be dominated by a helical hairpin arrangement that can move within the lipid bilayer in response to changes of membrane potential. These new structures force a re-evaluation of the structure-prediction problem.

What is missing from the present approach? One thing may be attention to the mechanisms of biological assembly. Constitutive α -helical MPs are as-

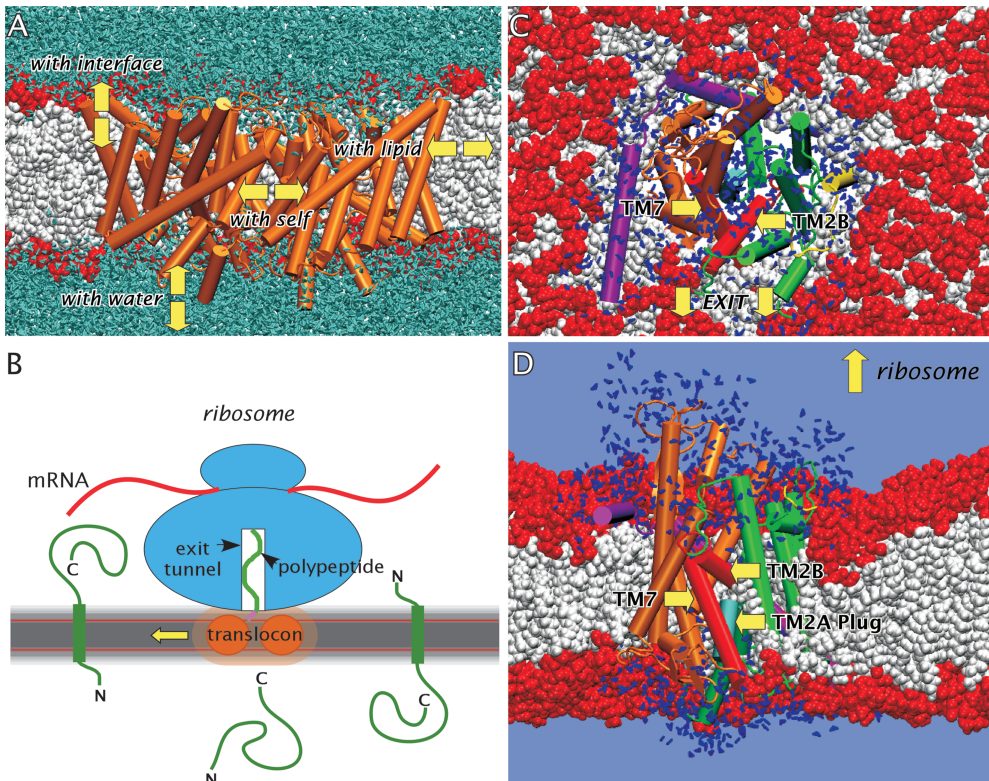


Fig. 1.1 Examples of MPs in lipid bilayers. In the molecular images, phospholipid head-groups are red and acyl chains are white. (A) An image of the CIC chloride channel [4, 111] embedded in a lipid bilayer (red and white) surrounded by water (aquamarine). The topology of this complex protein defies predictions using hydropathy plots. The yellow arrows highlight the components of the intrinsic interactions that must be understood quantitatively in order to predict the three-dimensional structure from the amino acid sequence. Intrinsic interactions are those involving the full-length polypeptide sequence, the lipid bilayer and water. The image was produced from a MD simulation of CIC in a POPC bilayer, courtesy of Dr. Alfredo Freitas at UC Irvine. (B) Schematic representation of the translocation or insertion of TM helices by a translocon receiving an elongating polypeptide chain from a ribosome. Polypeptide chains destined for translocation across the ER (center green chain) of eukaryotes or the plasma membrane of prokaryotes lack a segment of sufficient hydrophobicity and length to be identified by the translocon as a TM helix. The topology of a TM segment [112]

is determined by charge interactions [113] with the translocon complex (Sec61 in eukaryotes, SecY in bacteria). Several recent reviews discuss translocon-guided insertion of MPs [9–14, 114]. The schematic image is based upon Fig. 1 of [9]. (C and D) Structure of the SecY complex from *Methanococcus jannaschii* [7] that has been embedded in a POPC lipid bilayer using MD methods. A view of SecY normal to the bilayer plane looked at from the ribosome is shown in (C), while (D) shows a view along the bilayer plane looking into the so-called “gate” formed by helices TM2B and TM7. Nascent TM helices move into the bilayer through this gate. The translocon is in a closed state, because the structure was determined in the absence of an elongating polypeptide. The TM2A “plug helix” apparently seals the translocon in the absence of nascent peptide to prevent TM movement of ions. Waters within 5 Å of SecY are identified by the blue triangles. The images were prepared from a MD simulation, courtesy of Dr. Alfredo Freitas at UC Irvine. All molecular graphics images were produced using Visual Molecular Dynamics (VMD) [115].

sembled in membranes by means of a translocation/insertion process that involves physical engagement of a ribosome (Fig. 1.1 B) with the translocon complex [7–9] – itself a MP [9–12] (Fig. 1.1 C and D). Polypeptide segments destined for insertion as TM segments are identified by the translocon–bilayer system and shunted into the bilayer (reviewed in [9–15]). After release into the membrane’s bilayer fabric and disassembly of the ribosome–translocon machinery, a MP resides stably in a thermodynamic free energy minimum (evidence reviewed in [16, 17]). This outline of MP assembly suggests two fundamental categories of protein–lipid interactions that require consideration in structure-prediction algorithms: intrinsic and formative.

Intrinsic interactions are those responsible for the stability and structure of the full-length polypeptide chain after synthesis. These interactions, which produce the final shaping of MP structure, include interactions of the polypeptide chain with itself, water, the bilayer hydrocarbon core (HC), the bilayer interfaces (IFs) and, in some cases, cofactors (Fig. 1.1 A). Several recent reviews [17–21] provide extensive discussions of the evolution, structure and thermodynamic stability of MPs. An overview of intrinsic interactions that stabilize α -helical MPs is provided in Section 1.2. The basic thermodynamic principles of α -helical MPs, except for helix–helix interactions, apply also to β -barrel MPs, but this class of MPs will not be considered here. The interested reader should consult two excellent recent reviews on β -barrel MPs [21, 22].

The second category of interactions that require consideration in structure-prediction algorithms, formative interactions, involve interactions of elongating polypeptides with the translocon as well as the lipid bilayer. These interactions, which lead to the selection of a polypeptide segment for shunting into the bilayer, are the subject of Section 1.3. Recent experiments [23] have revealed the basic selection rules, and the recent structure of the bacterial (SecY) translocon [7, 8] (shown embedded in a lipid bilayer in Fig. 1.1 C and D) provides a structural context for the underlying formative interactions. The basic selection rules indicate that our understanding of the intrinsic interactions is incomplete.

1.2

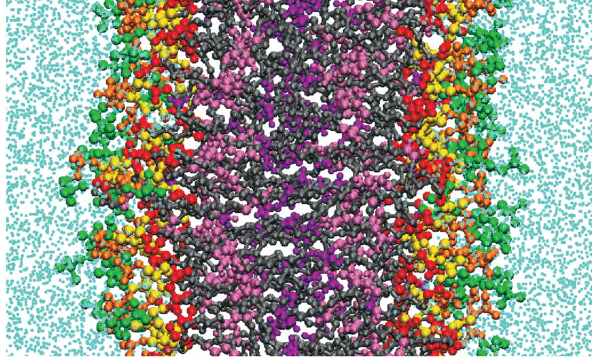
Membrane Proteins: Intrinsic Interactions

1.2.1

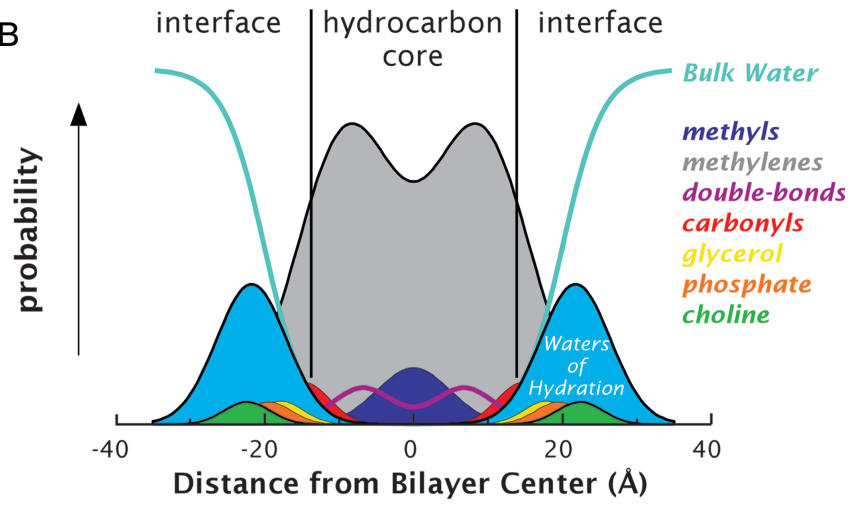
Physical Determinants of Membrane Protein Stability: The Bilayer Milieu

Two influences are paramount in shaping polypeptide structure in membranes. First, as indicated in Fig. 1.2, the membrane’s bilayer fabric has two chemically distinct regions: HC and IFs. IF structure and chemistry must be important because the specificity of protein signaling and targeting by membrane-binding domains could not exist otherwise [24], as discussed in detail in Chapters 15 to 17. Second, the high energetic cost of dehydrating the peptide bond, as when transferring it to a non-polar phase, causes it to dominate structure formation

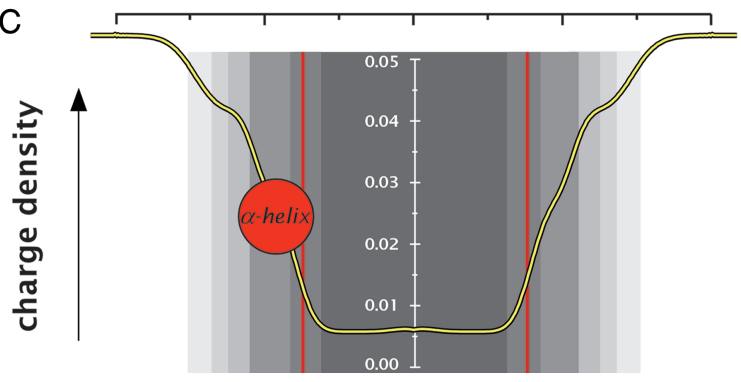
A



B



C



[25], as summarized in Fig. 1.3. The only permissible TM structural motifs of MPs are α -helices and β -barrels, because internal hydrogen bonding ameliorates this cost (see below).

As membranes must be in a fluid state for normal cell function, only the structure of fluid (L_α phase) bilayers is relevant to understanding how membranes mold proteins. However, atomic-resolution images of fluid membranes are precluded due to their high thermal disorder (Fig. 1.2A). Nevertheless, fundamental and useful structural information can be obtained from multilamellar bilayers (liquid crystals) dispersed in water or deposited on surfaces [26–29]. Their one-dimensional crystallinity perpendicular to the bilayer plane allows the distribution of matter along the bilayer normal to be determined by combined X-ray and neutron diffraction measurements (liquid crystallography; reviewed in [30, 31]). The resulting “structure” consists of a collection of time-averaged probability distribution curves of water and lipid component groups (carbonyls, phosphates, etc.), representing projections of three-dimensional motions onto the bilayer normal. Fig. 1.2B shows the liquid-crystallographic structure of an L_α phase dioleoylphosphatidylcholine (DOPC) bilayer [32].

Three features of this structure are important. First, the widths of the probability densities reveal the great thermal disorder of fluid membranes. Second, the combined thermal thickness of the IFs (defined by the distribution of the waters of hydration) is approximately equal to the 30-Å thickness of the HC. The thermal thickness of a single IF (around 15 Å) can easily accommodate an α -helix parallel to the membrane plane. The common cartoons of bilayers that assign a diminutive thickness to the bilayer IFs are thus misleading. Third, the thermally disordered IFs are highly heterogeneous chemically. A polypeptide chain in an IF must experience dramatic variations in environmental polarity

Fig. 1.2 The liquid-crystalline structure of a fluid DOPC bilayer.

(A) Molecular graphics image of DOPC taken from a MD simulation by Ryan Benz at UC Irvine. The color scheme for the component groups (carbonyls, phosphates, water, etc.) is given in (B). The image was prepared by S. White using VMD [115].

(B) Liquid-crystallographic structure of a fluid DOPC lipid bilayer [32]. The “structure” of the bilayer is comprised of a collection of transbilayer Gaussian probability distribution functions representing the lipid components that account for the entire contents of the bilayer unit cell. The areas under the curves correspond to the number of constituent groups per lipid represented by the distributions (one phosphate, two carbonyls, four methyls, etc.). The widths of the Gaussians

measure the thermal motions of the lipid components and are simply related to crystallographic B factors [39, 40, 116]. The thermal motion of the bilayer is extreme: lipid-component B factors are typically around 150 \AA^2 , compared to around 30 \AA^2 for atoms in protein crystals.

(C) Polarity profile (yellow curve) of the DOPC bilayer (above) computed from the absolute values of atomic partial charges [33]. The end-on view in (B) of an α -helix with diameter $\sim 10 \text{ \AA}$ – typical for MP helices [87] – shows the approximate location of the helical axes of the amphipathic-helix peptides Ac-18A-NH₂ [40] and melittin [39], as determined by a novel, absolute-scale X-ray diffraction method (reviewed in [117]). Panels (B) and (C) have been adapted from reviews by White and Wimley [17, 33, 118].

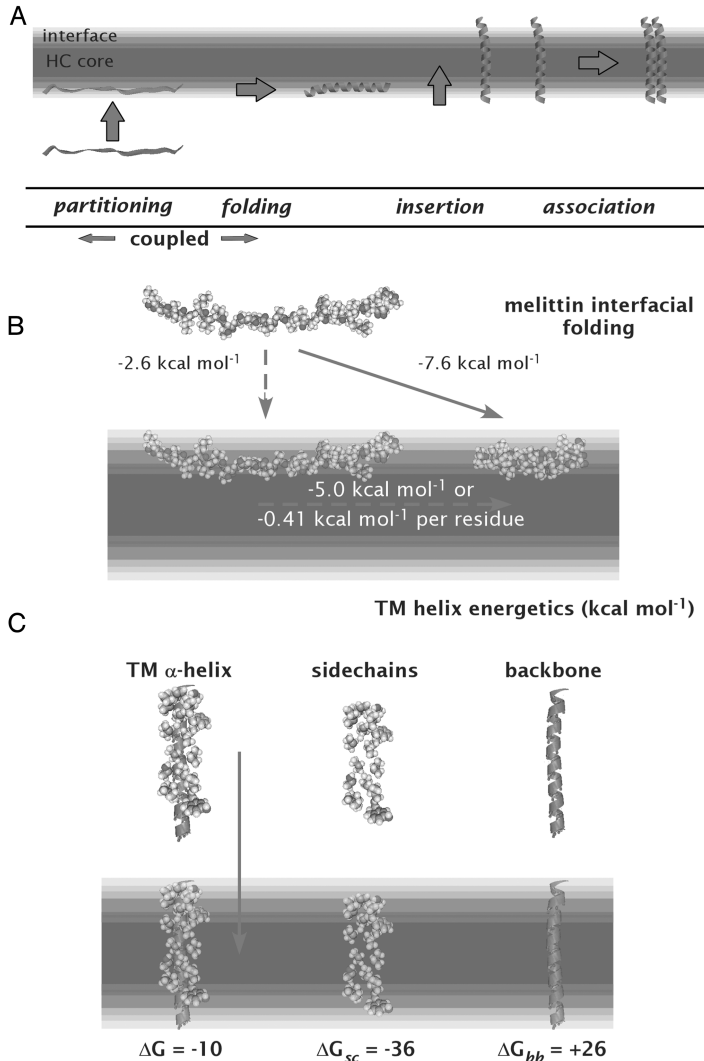


Fig. 1.3 Energetics of peptide interactions with lipid bilayers.

(A) Schematic representation of the shaping of protein structure through polypeptide–bilayer interactions. Based upon the four-step thermodynamic cycle of Wimley and White [17] for describing the partitioning, folding, insertion and association of α -helical polypeptides. The aqueous insolubility of MPs, folded or unfolded, precludes direct determinations of interaction free energies. The only route to understanding the energetics of MP stability is through studies

of small, water-soluble peptides [62, 64, 65, 68]. The association of TM helices is probably driven by van der Waals interactions, giving rise to knob-into-hole packing [84–86, 119]. The GxxxG motif is especially important in helix–helix interactions in membranes [90, 91].

(B) Energetics of secondary structure formation by melittin at the bilayer IF [65]. Unfolded peptides are driven toward the folded state in the IF because hydrogen-bond formation dramatically lowers the cost of peptide-bond partitioning, which is the

over a short distance due to the steep changes in chemical composition, as illustrated by the yellow curve in the lower half of Fig. 1.2C [33]. As the regions of first contact, the IFs are especially important in the folding and insertion of non-constitutive MPs, such as diphtheria toxin [34, 35] and to the activity of surface-binding enzymes, such as phospholipases [36–38]. However, for reasons discussed below, they are also likely to be important in translocon-assisted folding of MPs.

Experimentally determined bilayer structures such as the one in Fig. 1.2C are essential for understanding thermodynamic measurements of peptide–bilayer interactions at the molecular level. Recent extension of the liquid-crystallographic methods to bilayers containing peptides such as melittin [39] and other amphipathic peptides [40] makes this a practical possibility. However, there are numerous other X-ray and neutron diffraction approaches that provide important information about the molecular interactions of peptides with lipid bilayers [41–47]. Molecular dynamics (MD) simulations of bilayers [48–51] (Fig. 1.2A) are rapidly becoming an essential structural tool for examining lipid–protein interactions at the atomic scale [52–57]. The future offers the prospect of combining bilayer diffraction data with MD simulations in order to arrive at experimentally validated MD simulations of fluid lipid bilayers [58]. This approach should allow one to convert the static one-dimensional images obtained by diffraction (Fig. 1.2B) into dynamic, three-dimensional structures for examining peptide–lipid interactions in atomic detail.

1.2.2

Physical Determinants of Membrane Protein Stability: Energetics of Peptides in Bilayers

Experimental exploration of the stability of intact MPs is problematic due to their general insolubility. One approach to stability is to “divide and conquer” by



dominant determinant of whole-residue partitioning. The free energy reduction accompanying secondary structure formation by melittin is around $0.4 \text{ kcal mol}^{-1}$ per residue [64, 65], but may be as low as $0.1 \text{ kcal mol}^{-1}$ for other peptides [120]. Although small, such changes in aggregate can be large. For example, the folding of 12 residues of 26-residue melittin into an α -helical conformation causes the folded state to be favored over the unfolded state by around 5 kcal mol^{-1} . To put this number in perspective, the ratio of folded to unfolded peptide is around 4700.

(C) The energetics of TM helix insertion based upon the work of Wimley and White [68] and Jayasinghe et al. [72]. Estimated relative free energy contributions of the side-chains (ΔG_{sc}) and backbone (ΔG_{bb}) to the helix-insertion energetics of glycoprotein A [73]. The net side-chain contribution (relative to glycine) was computed using the *n*-octanol hydrophobicity scale of Wimley et al. [74]. The per-residue cost of partitioning a polyglycine α -helix is $+1.15 \text{ kcal mol}^{-1}$ [72]. (Adapted from reviews by White et al. [19] and White [20]).

studying the membrane interactions of fragments of MPs, i.e. peptides. Because MPs are equilibrium structures, one is free to describe the interactions by any convenient set of experimentally accessible thermodynamic pathways, irrespective of the biological synthetic pathway. One particularly useful set of pathways is the so-called four-step model [17] (Fig. 1.3 A), which is a logical combination of the early three-step model of Jacobs and White [59] and the two-stage model of Popot and Engelman [60], in which TM helices are first “established” across the membrane and then assemble into functional structures (helix association; reviewed in [61]). Although these pathways do not mirror the actual biological assembly process of MPs, they are nevertheless useful for guiding biological experiments, because they provide a thermodynamic context within which biological processes must proceed.

In the four-step model (Fig. 1.3 A), the free energy reference state is taken as the unfolded protein in an IF. However, this state cannot actually be achieved with MPs because of the solubility problems. Nor can it be achieved with small non-constitutive membrane-active peptides, such as melittin, because binding usually induces secondary structure (partitioning-folding coupling). It can be defined for phosphatidylcholine (PC) IFs by means of an experiment-based interfacial free energy (hydrophobicity) scale [62] derived from partitioning into 1-palmitoyl-2-oleoyl-phosphatidylcholine (POPC) bilayers of tri- and pentapeptides [59, 62] that have no secondary structure in the aqueous or interfacial phases. This scale (Fig. 1.4 A), which includes the peptide bonds as well as the side-chains, allows calculation of the virtual free energy of transfer of an unfolded chain into an IF. For peptides that cannot form regular secondary structure, such as the antimicrobial peptide indolicidin, the scale predicts observed free energies of transfer with remarkable accuracy [63]. This validates it for computing virtual partitioning free energies of proteins into PC IFs. Similar scales are needed for other lipids and lipid mixtures.

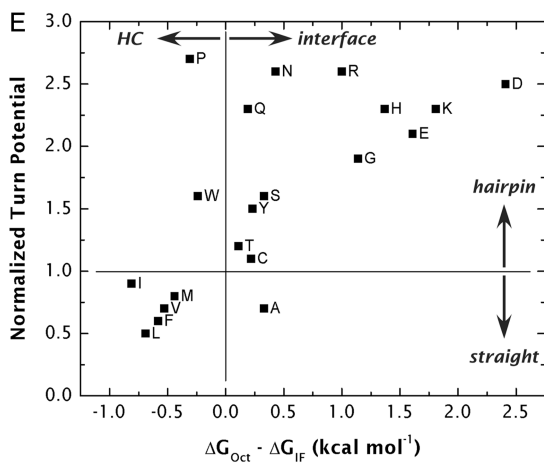
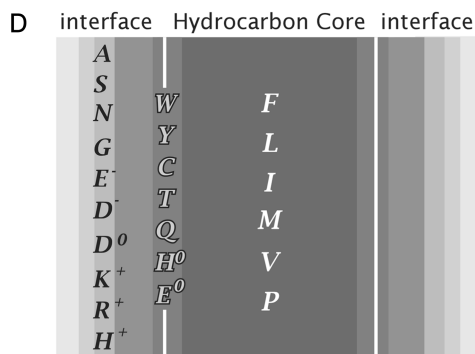
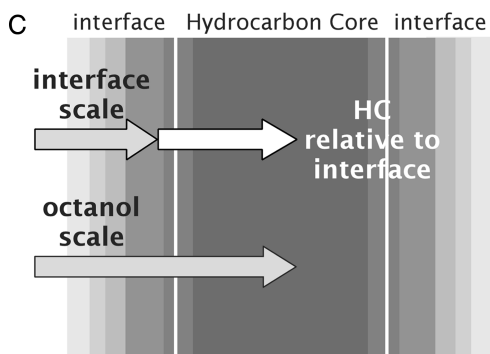
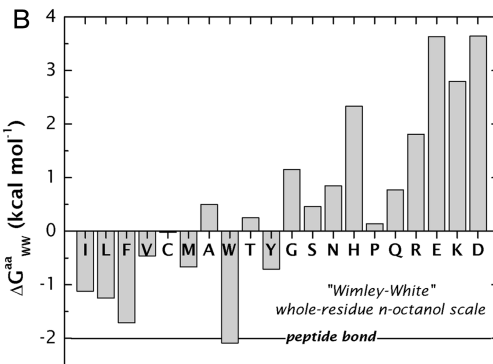
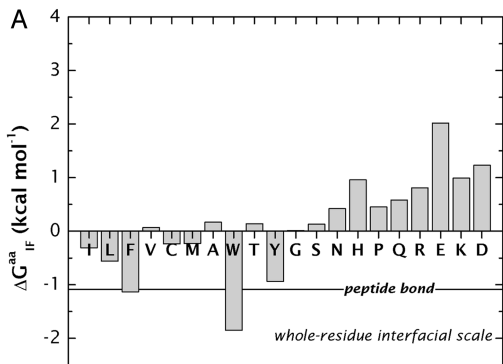
The high cost of interfacial partitioning of the peptide bond [62], $1.2 \text{ kcal mol}^{-1}$, explains the origin of partitioning-folding coupling and it also explains why the IF is a potent catalysis of secondary structure formation. Wimley et al. [64] showed for interfacial β -sheet formation that hydrogen-bond formation reduces the cost of peptide partitioning by about $0.5 \text{ kcal mol}^{-1}$ per peptide bond. The folding of melittin into an amphipathic α -helix on POPC membranes involves a per-residue reduction of about $0.4 \text{ kcal mol}^{-1}$ [65] (Fig. 1.3 B). The folding of other peptides may involve smaller per-residue values [66, 67]. The cumulative effect of these relatively small per-residue free energy reductions can be very large when tens or hundreds of residues are involved.

The energetics of TM helix stability also depend critically on the partitioning cost of peptide bonds (Fig. 1.3 C). Determination of the energetics of TM α -helix insertion, which is necessary for predicting structure, is difficult because non-polar helices tend to aggregate in both aqueous and interfacial phases [68]. The broad energetic issues are clear [69], however. Computational studies [70, 71] suggest that the transfer free energy ΔG_{CONH} of a non-hydrogen-bonded peptide bond from water to alkane is $+6.4 \text{ kcal mol}^{-1}$, compared to only $+2.1 \text{ kcal mol}^{-1}$

for the transfer free energy ΔG_{Hbond} of a hydrogen-bonded peptide bond. The per-residue free energy cost of disrupting hydrogen bonds in a membrane is therefore about 4 kcal mol^{-1} . A 20-amino-acid TM helix would thus cost 80 kcal mol^{-1} to unfold within a membrane, which explains why unfolded polypeptide chains cannot exist in a TM configuration.

As discussed in detail elsewhere [19, 72], ΔG_{Hbond} sets the threshold for TM stability as well as the so-called decision level in hydrophathy plots [2]. The free energy of transfer of non-polar side-chains dramatically favors helix insertion, while the transfer cost of the helical backbone dramatically disfavors insertion. For example [19], the favorable (hydrophobic effect) free energy for the insertion of the single membrane-spanning helix of glycoporphin A [73] is estimated to be $-36 \text{ kcal mol}^{-1}$, whereas the cost ΔG_{bb} of dehydrating the helix backbone is $+26 \text{ kcal mol}^{-1}$ (Fig. 1.3C). The net free energy ΔG_{TM} favoring insertion is thus $-10 \text{ kcal mol}^{-1}$. As is common in so many biological equilibria, the free energy minimum is the small difference of two relatively large opposing energetic terms. Uncertainties in the per-residue cost of backbone insertion will have a major effect on estimates of TM helix stability, the interpretation of hydrophathy plots, and the establishment of the minimum value of side-chain hydrophobicity required for stability. An uncertainty of $0.5 \text{ kcal mol}^{-1}$, for example, would cause an uncertainty of about 10 kcal mol^{-1} in ΔG_{TM} !

What is the most likely estimate of ΔG_{Hbond} ? The practical number is the cost $\Delta G_{\text{glycyl}}^{\text{helix}}$ of transferring a single glycyl unit of a polyglycine α -helix into the bilayer HC. Electrostatic calculations [71] and the octanol partitioning study of Wimley et al. [74] suggested that $\Delta G_{\text{glycyl}}^{\text{helix}} = +1.25 \text{ kcal mol}^{-1}$, which is the basis for the calculation of ΔG_{bb} . The cost of transferring a random-coil glycyl unit into *n*-octanol [74] is $+1.15 \text{ kcal mol}^{-1}$, which suggested that the *n*-octanol whole-residue hydrophobicity scale [17] (Fig. 1.4B) derived from partitioning data of Wimley et al. [74] might be a good measure of $\Delta G_{\text{glycyl}}^{\text{helix}}$. This hypothesis was borne out by a study [72] of known TM helices cataloged in the MPtopo database of MPs of known topology [75], accessible via <http://blanco.biomol.uci.edu/mptopo>. This study showed that $+1.15 \text{ kcal mol}^{-1}$ is indeed the best estimate of $\Delta G_{\text{glycyl}}^{\text{helix}}$. Using this value, TM helices for MPs of known three-dimensional structure could be identified with high accuracy in the 2001 edition of MPtopo. This scale also includes free energy values for protonated and deprotonated forms of Asp, Glu and His. In addition, Wimley et al. [76] determined the free energies of partitioning salt-bridges into octanol, which are believed to be good estimates for partitioning into membranes [72]. This has led to the augmented Wimley–White (aWW) hydrophobicity scale [72] that forms the basis for a useful hydrophathy-based tool, MPEx, for analyzing MP protein stability. MPEx is available as an on-line java applet at <http://blanco.biomol.uci.edu/mpex>. However, the scale fails miserably in the prediction of the topology of the ClC chloride channel (Fig. 1.1A), indicating the need to understand the translocon-assisted folding of MPs. Nevertheless, the WW experiment-based whole-residue hydrophobicity scales [62, 72, 74], Fig. 1.4 [A (ΔG_{IF}) and B (ΔG_{WW} or ΔG_{Oct})], provide a solid starting point for understanding the physical stability of MPs. The



whole-residue WW scale provides an important connection between physical chemistry and biology (see below).

When the two scales are used together (Fig. 1.4 C), one can estimate the preference of a polypeptide segment for the HC as an α -helix relative to the membrane IF as an unfolded chain. The “octanol–IF” scale, $\Delta G_{\text{oct-IF}} = \Delta G_{\text{oct}} - \Delta G_{\text{IF}}$, divides the amino acid residues into three groups (Fig. 1.4 D): strongly IF preferring, strongly HC preferring and those that are borderline ($|\Delta G_{\text{oct-IF}}| \leq 0.25 \text{ kcal mol}^{-1}$). The octanol–IF scale provided insights into translocon-assisted folding [77–79] and was the stimulus for undertaking a detailed examination of the recognition of TM helices by the endoplasmic reticulum (ER) translocon (see below) [23].

1.2.3

Physical Determinants of Membrane Protein Stability: Helix–Helix Interactions in Bilayers

The hydrophobic effect is generally considered to be the major driving force for compacting soluble proteins [80]. However, it cannot be the force driving compaction (association) of TM α -helices. Because the hydrophobic effect arises solely from dehydration of non-polar surfaces [81], it is expended after helices are established across the membrane. Helix association is most likely driven primarily by van der Waals forces; more specifically, the London dispersion force (reviewed in [17, 18]). But why would van der Waals forces be stronger between helices than between helices and lipids?

Extensive work [82–86] on dimer formation of glycoporphin A in detergents reveals the answer: knob-into-hole packing that allows more efficient packing between helices than between helices and lipids. Tight, knob-into-hole packing has been found to be a general characteristic of helical-bundle MPs as well [87,

Fig. 1.4 Summary of experiment-based hydrophobicity scales that are useful for understanding MP stability and translocon-assisted folding. (A) The WW interfacial hydrophobicity scale determined from measurements of the partitioning of short peptides into phosphatidylcholine vesicles [62]. (B) The WW octanol hydrophobicity scale determined from the partitioning of short peptides into *n*-octanol [74] that predicts the stability of TM helices [72]. The free energy values along the abscissa are ordered in the same manner as in Fig. 1.6 A. (C) The basis for deriving the octanol–IF scale ($\Delta G_{\text{oct-IF}} = \Delta G_{\text{oct}} - \Delta G_{\text{IF}}$) from the scales shown in (A and B). Numerical values for all of the scales can be obtained at [\[blanco.biomol.uci.edu/hydrophobicity_scales.html\]\(http://blanco.biomol.uci.edu/hydrophobicity_scales.html\).](http://</p>
</div>
<div data-bbox=)

(D) The $\Delta G_{\text{oct-IF}}$ scale divides the natural amino acid residues into three classes based upon their relative propensities for the HC and the membrane IF.

(E) A plot of the normalized turn propensity for helical hairpin formation [78] versus the octanol–IF hydrophobicity scale. There is a clear correlation between the turn propensity and $\Delta G_{\text{oct-IF}}$ hydrophobicity. Those residues that favor the conversion of a long (about 40 amino acids), single-spanning poly-leucine TM helix into a helical hairpin (two TM helices separated by a tight turn) are generally the same ones that favor the membrane IF. See text for discussion.

(Adapted from a review by White [20]).

88]. For glycoporphin A dimerization, knob-into-hole packing is facilitated by the GxxxG motif, in which the glycines permit close approach of the helices. The substitution of larger residues for glycine prevents the close approach and, hence, dimerization [82, 85, 86]. The so-called TOX-CAT method [89] has made it possible to sample the amino acid motifs preferred in helix-helix association in biological membranes by using randomized sequence libraries [90]. The GxxxG motif is among a significant number of motifs that permit close packing. A statistical survey of MP sequences disclosed that these motifs are very common in MPs [91].

Dimerization studies of glycoporphin in detergent micelles [85] do not permit the absolute free energy of association to be determined, because of the large free energy changes associated with micelle stability. However, estimates [17] suggest 1–5 kcal mol⁻¹ as the free energy cost of separating a helix from a helix bundle within the bilayer environment. The cost of breaking hydrogen bonds within the bilayer HC (above) implies that hydrogen bonding between α -helices could provide a strong stabilizing force for helix association. This is borne out by recent studies of synthetic TM peptides designed to hydrogen bond to one another [92, 93]. Interhelical hydrogen bonds, however, are not common in MPs (reviewed in [17]). Indeed, lacking the specificity of knob-into-hole packing, they could be hazardous because of their tendency to cause promiscuous aggregation [18], although they are probably important in the association of TM signaling proteins [94].

1.3

Membrane Proteins: Formative Interactions

1.3.1

Connecting Translocon-assisted Folding to Physical Hydrophobicity Scales: The Interfacial Connection

The literature on translocon-assisted MP folding has been reviewed extensively in the past several years [9–14]. Here it is sufficient to note that the signal recognition particle (SRP) targets nascent ribosome-bound membrane and secreted proteins to the translocon complex (Sec61 in eukaryotes, SecY in bacteria), whereupon membrane integration and folding occurs, provided that the nascent protein has at least one run of amino acids with sufficient hydrophobicity to form a TM helix/stop-transfer sequence (Fig. 1.1 B). Otherwise, the protein is secreted across the membrane. An important topic, reviewed elsewhere [9, 95, 96], is the physical basis for topology determination of the initial TM segment.

There have been two points of view about translocon-assisted membrane integration, discussed extensively by Johnson [14]. The “sequential” point-of-view visualizes the translocon as having a large-diameter tunnel (around 50 Å) into which the nascent protein chain is secreted during folding, in preparation for insertion into the lipid bilayer via a passageway through the wall of the translocon. A crucial feature of this scheme is that the ribosome must make a tight seal with the translocon in order to prevent ion leakage. There is a growing body of evidence, however,

that the alternate “concerted” scheme, in which the translocon complex and the lipid work together, is more likely (reviewed in [9]). Two low-resolution (around 15 Å) images of ribosome–translocon assemblies indicate significant gaps between the ribosome and translocon [97, 98], which eliminates the possibility of a tight seal. It appears that sealing must be provided in some way by the nascent peptide within the translocon itself. The structure of an archaeal SecY translocon, composed of 10 TM segments, strongly supports this view (Fig. 1.1 C and D). The nascent TM segment apparently emerges laterally through a gate formed principally by helices TM2B and TM7. A short “plug” helix (TM2A) serves to seal the translocon in the absence of a nascent chain. Site-specific photo-cross-linking studies [99] show that the nascent chain can cross-link with lipids well before the termination of translation, implying that the growing chain interacts with both the translocon and neighboring lipids during folding. Heinrich et al. [100] concluded that the integration of TM domains occurs through a lipid-partitioning process as a result of the TM segment being in contact with the lipid as soon as it arrives in the translocon channel. However, integration into the membrane can occur only if a polypeptide segment has the right properties, such as sufficient hydrophobicity.

What is the minimum hydrophobicity required for a 20-amino-acid stop-transfer segment to be integrated into the lipid bilayer? Chen and Kendall [101] examined this question for *Escherichia coli* by attaching artificial stop-transfer sequences to alkaline phosphatase, which is a water-soluble protein that is normally secreted across the membrane. Potential stop-transfer sequences (21 amino acids) composed of Leu and Ala in various ratios were introduced into an internal position of the enzyme by cassette mutagenesis. The threshold value of hydrophobicity for integration was found to be 16 Ala and five Leu. This is exactly the threshold predicted by the WW octanol-based hydrophobicity scale, as shown by Jayasinghe et al. [72]. This establishes a close relationship between the WW octanol scale and translocon-assisted TM helix insertion.

There is also indirect evidence for a relationship between interfacial hydrophobicity and translocon-mediated folding. Nilsson and von Heijne [102] made the interesting observation that a Leu39Val hydrophobic sequence introduced into leader peptidase was incorporated into the membranes of dog pancreas microsomes as a single TM helix. The fact that this helix is twice the length of the typical TM helix strongly supports the idea of early contact of the growing chain with membrane lipids. The more striking observation, however, was that the introduction of a single proline into the center of the Leu39Val segment caused it to be inserted as a helical hairpin. That is, the proline induced the formation of two TM segments separated by a tight turn. Expanding on this observation, Monné et al. [77, 78] established a turn-propensity scale by introducing one or two of each of the natural amino acids into the center of a 40-residue poly-leucine sequence. The residues with a favorable turn potential were found to be, in decreasing order, Pro, Asn, Arg, Asp, His, Gln, Lys, Glu and Gly. Except for Pro, which commonly occurs within TM helices of ordinary length [103], these are the residues in the WW $\Delta G_{\text{oct-IF}}$ scale (Fig. 1.4 D) that have a strong IF preference. Another misfit is Ala, which has a low turn potential but a significant

interfacial preference. The relationship between turn potential and the octanol-IF scale is shown in Fig. 1.4E. The correlation coefficient between the scales is 0.67, meaning that there is not a strict linear relationship. This is not surprising because turn potential is affected by the length of the long polyleucine segment and the number of residues of a given type introduced into the segment's center [78]. For example, unlike the Leu39Val, a single proline placed in the center of a Leu29Val sequence does not induce hairpin formation.

A closer connection between turn potential and the WW $\Delta G_{\text{oct-IF}}$ scale was disclosed by studies of turn induction by runs of Ala residues placed in the center of polyleucine segments [79]. A run of around four alanines was found to induce helical hairpins efficiently in hydrophobic segments as short as 34 residues. Furthermore, glycosylation mapping revealed a slight preference of alanine for the membrane IF, consistent with the WW $\Delta G_{\text{oct-IF}}$ scale.

These various studies support the idea that the translocon and lipid bilayer work in concert to integrate hydrophobic segments into membranes, which strengthens the lipid-partitioning model of Rapoport et al. [100]. In addition, the studies establish a direct link between physical hydrophobicity scales and translocon-assisted folding. An early study [104] of the relationship between biophysical hydrophobicity and translocon-mediated integration found that popular hydrophobicity scales of the time could not accurately predict the hydrophobic threshold for stop-transfer activity. The reason is now understood [72]. Prior to the WW experiment-based whole-residue scales, no hydrophobicity scale took into account the cost of dehydrating the helix backbone. As result, side-chain-only scales dramatically over-predict TM helices in MPs of known structure. If one thinks of the threshold for insertion as the mid-point of a Boltzmann probability curve (see below), side-chain-only scales will cause the apparent threshold to have a positive ΔG , rather than the expected value of zero. Indeed, Sääf et al. [104] found the mean per-residue hydrophobicity threshold to be approximately $+1.5 \text{ kcal mol}^{-1}$, which is about the cost of dehydrating the peptide bond. Had the partitioning cost of the peptide bond been appreciated at the time and taken into account, the threshold then would have been very close to $\Delta G=0$. With the availability of experiment-based physical scales that account reasonably well for both interfacial and HC partitioning, it became possible to design more finely tuned TM helices for probing translocon-assisted folding [23], described below.

1.3.2

Connecting Translocon-assisted Folding to Physical Hydrophobicity Scales: Transmembrane Insertion of Helices

Important new insights into TM helix insertion have been obtained by Hessa et al. [23] using an *in vitro* expression system [104] that permits quantitative assessment of the membrane insertion efficiency of model TM segments. Specifically, they examined the integration into membranes of dog pancreas rough microsomes of designed polypeptide segments. These segments were engineered into the luminal P2 domain of the integral MP leader peptidase (Lep) (Fig. 1.5A–C).

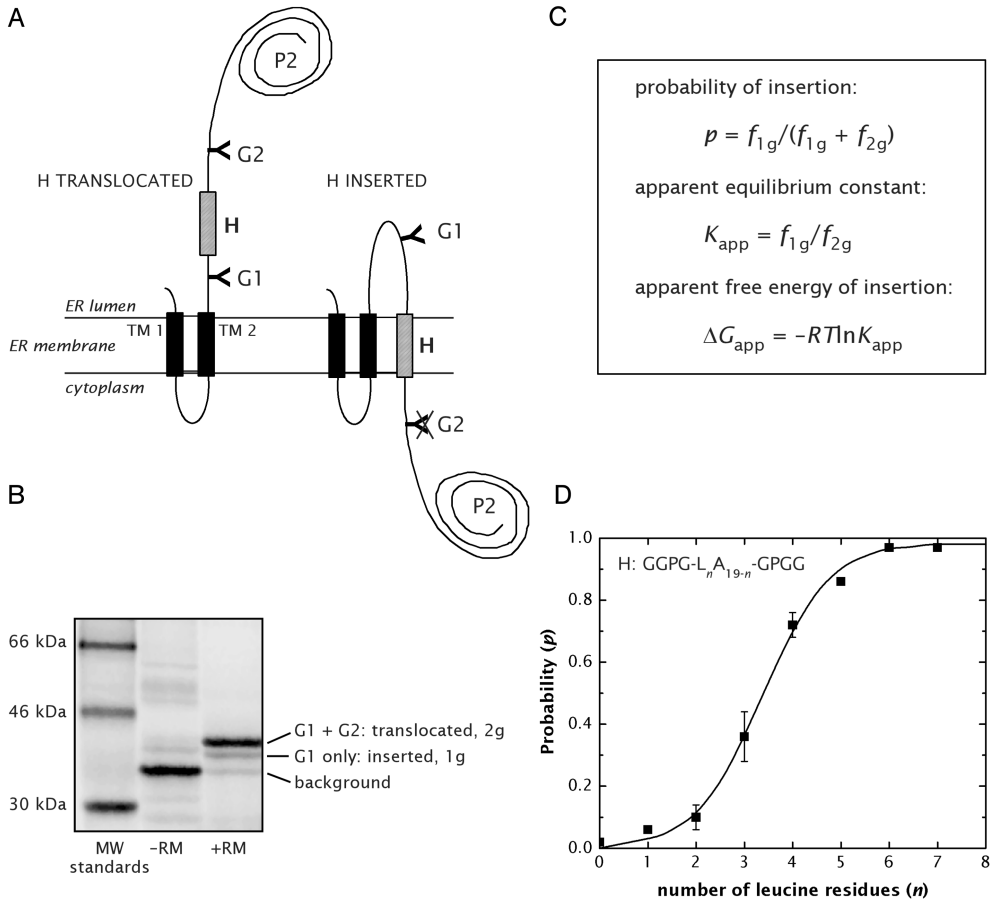


Fig. 1.5 Integration of designed TM segments (H-segments) into the ER using dog pancreas microsomal membranes. This system was used to explore systematically the hydrophobicity requirements for TM helix integration via the Sec61 translocon [23]. (A) Wild-type leader peptidase (Lep) from *E. coli* has two N-terminal TM segments (TM1 and TM2) and a large luminal domain (P2). H-segments were inserted between residues 226 and 253 in the P2 domain. Glycosylation acceptor sites (G1 and G2) were placed in positions flanking the H-segment. For H-segments that integrate into the membrane, only the G1 site is glycosylated (right), whereas both the G1 and G2 sites are glycosylated for H-segments that do not integrate into the membrane (left). (Based upon Hessa et al. [23]).

(B) An example of sodium dodecylsulfate gels used in the determination of the extent of glycosylation of Lep/H-segment constructs. Plasmids encoding the Lep/H-segment constructs were transcribed and translated *in vitro* in the absence (–RM) and presence (+RM) of dog pancreas rough microsomes. Data from Hessa et al. [23]. (C) Equations used by Hessa et al. [23] for the analysis of gels of the type shown in (B). (D) Mean probability of insertion, p , for H-segments with $n=0-7$ Leu residues in H-segments of the form GGPG-(L_{*n*}A_{*19-n*})-GPGG. The curve is the best-fit Boltzmann distribution, which suggests equilibrium between the inserted and translocated H-segments. (Data re-plotted from Hessa et al. [23]).

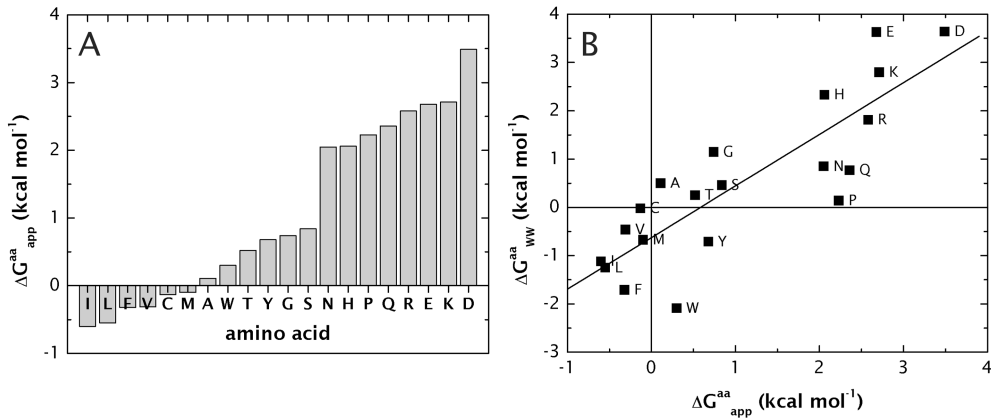


Fig. 1.6 Biological and biophysical hydrophobicity scales.

(A) ΔG_{app}^{aa} scale derived by Hessa et al. [23] from H-segments (Fig. 1.5) with the indicated amino acid placed in the middle of the 19-residue hydrophobic stretch.

(B) Correlation between ΔG_{app}^{aa} and the WW water/octanol free energy scale (ΔG_{WW}^{aa}) (Fig. 1.4B). (Data re-plotted from Hessa et al. [23]).

The first step in the analysis was to test the hypothesis that the WW octanol scale had correctly identified the minimum hydrophobicity required for TM helix stability. Initial measurements were thus made by testing H-segments of the design GGPG-(L_nA_{19-n})-GPGG with $n=0-7$. As shown in Fig. 1.5D, the probability of insertion, $p(n)$, conforms accurately to a Boltzmann distribution, which shows that translocon-mediated insertion has the appearance of an equilibrium process.

A “biological” hydrophobicity scale (ΔG_{app}^{aa}) could be derived from studies on H-segments in which each of the 20 naturally occurring amino acids were placed in the middle position of the segment. As seen in Fig. 1.6A, Ile, Leu, Phe and Val promote membrane insertion ($\Delta G_{app}^{aa} < 0$), Cys, Met and Ala have $\Delta G_{app}^{aa} \sim 0$, and all polar and charged residues have $\Delta G_{app}^{aa} > 0$. The correlation between the ΔG_{app}^{aa} scale and the WW octanol scale is shown in Fig. 1.6B. Considering the complexity of the biological system, the two scales correlate surprisingly well. The overall high correspondence between the two scales indicates that the recognition of TM segments by the translocon involves direct interaction between the segment and the surrounding lipid [100].

The ΔG_{app}^{aa} biological scale is strictly valid only for residues placed in the middle of the H-segment. To explore the role of residue position, Hessa et al. also performed symmetric “scans” in which a pair of residues of a given kind were moved symmetrically from the center of the H-segment towards its N- and C-termini. The results are summarized in Fig. 1.7A – while the contributions from apolar residues do not vary much with position within the H-segment, Trp and Tyr strongly reduce membrane insertion when placed centrally, but be-

come much less unfavorable as they are moved apart. This positional dependence is even stronger for charged residues such as Lys and Asp. The positional effects are consistent with the relative preferences of Trp, Tyr and charged residues for the bilayer IF (Fig. 1.4), suggesting the importance of interactions of elongating peptides with the lipid bilayer.

The position dependence observed by Hessa et al. [23] had another important characteristic. Namely, the probability of helix insertion was sensitive to amphiphilicity of the elongating peptide as an α -helix (Fig. 1.7B). Helices with a low hydrophobic moment [105] had a higher insertion probability than those with a high hydrophobic moment, as though the polar surface had a more favorable interaction energy with the translocon than the non-polar surface.

Overall, the results of Hessa et al. [23] suggest that direct protein–lipid interactions are essential for the recognition of TM helices by the translocon, and support models based on a partitioning of the TM helices between the Sec61 translocon and the surrounding lipid. The details of the partitioning process remain to be determined, but presumably the open state of the translocon is a highly dynamic one that permits rapid sampling of the translocon–bilayer IF by the translocating polypeptide. The results also provide a starting point for quantitative modeling of the membrane insertion of TM segments. However, Hessa et al. caution that the base $\Delta G_{\text{app}}^{\text{aa}}$ scale alone (Fig. 1.6A) is not appropriate for calculating membrane insertion efficiency of natural polypeptide segments because of the strong positional dependence of $\Delta G_{\text{app}}^{\text{aa}}$.

The importance of including the position dependence was especially apparent in a related study by Hessa et al. [106] of the TM insertion of the voltage sensor of the KvAP voltage-gated potassium channel [6]. The critical element in the sensor domains in virtually all voltage-gated ion channels is the S4 helix, which contains at least four regularly spaced Arg residues interspersed with hydrophobic residues. Voltage activation has been suggested to involve movement of S4 through the lipid bilayer in response to membrane depolarization [107]. This mechanism is controversial, because of the presumed cost of burying charges in the HC of the lipid bilayer [108]. To examine this issue, Hessa et al. [106] measured the insertion efficiency of an H-segment containing the arginine-rich region of the KvAP S4 helix (Fig. 1.7C). The measured ΔG_{app} was found to be only $0.5 \text{ kcal mol}^{-1}$ rather than the value of $3.9 \text{ kcal mol}^{-1}$ computed from the biological hydrophobicity scale (Fig. 1.6A). However, when measurements of the position dependence of $\Delta G_{\text{app}}^{\text{Arg}}$ were taken into account, the computed value of ΔG_{app} agreed closely with the measured value. The position dependence of $\Delta G_{\text{app}}^{\text{aa}}$ is clearly extremely important. However, it is surprising, because the HC of the bilayer has always been assumed to behave as a uniform alkyl liquid.

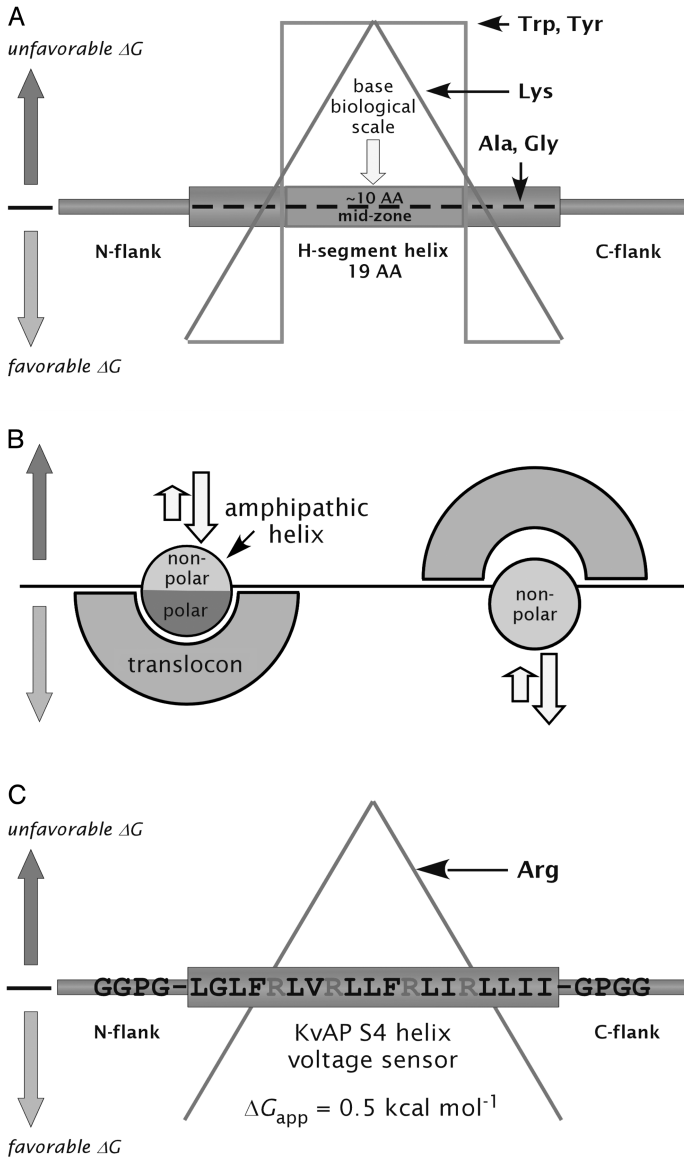


Fig. 1.7

1.4 Perspectives

The lipid bilayer presents a complex environment for the folding and stability of MPs. Much progress has been made in describing and understanding this environment, and in teasing out the basic thermodynamic principles of its interactions with peptides. Yet, despite our progress with model systems, our understanding of the details of protein–lipid interactions *in vivo* remain woefully inadequate, as revealed by the studies of translocon-assisted insertion of TM helices [23, 106]. The dogma of the past 25 years or so has been that the HC of the lipid bilayer is simply a thin alkyl film that is strictly off-limits to charged amino acids because of the Born charging energy [109]. It has certainly dominated thinking about the energetics of ion channel voltage sensors [108].

The new information that has emerged from the studies of translocon-assisted protein folding tells us that the lipid bilayer has greater possibilities for lipid–protein interactions than previously thought. The dependence of the insertion energetics of polar residues on position within TM helices reveals this most clearly. The ease with which the S4 helix of the KvAP potassium channel voltage sensor can be inserted across the ER membrane seems astounding at first. However, in the context of diphtheria toxin, the result is not so surprising. The T-domain of diphtheria toxin is capable, on its own, of translocating large portions of itself (including highly charged helices) and the water-soluble catalytic domain across endosomal membranes spontaneously in response to lowered pH [110]. Just how this can be accomplished is a mystery that may, at its core, be related to the high structural integrity of the lipid bilayer, an integrity that

Fig. 1.7 Summary of the basic code used by the ER translocon to identify TM segments based upon the findings of Hessa et al. [23, 106]. As noted in Fig. 1.6, the biological $\Delta G_{\text{app}}^{\text{aa}}$ scale is based upon values obtained from amino acids placed in the center of the H-segment. The results of Hessa et al. reveal very strong dependences upon amino acid position, contrary to the implicit assumption of hydrophathy plot analyses that the position of an amino acid within a bilayer-spanning helix does not matter.

(A) The $\Delta G_{\text{app}}^{\text{aa}}$ values for some amino acids such as Gly and Ala are little affected by position within the TM segment. The $\Delta G_{\text{app}}^{\text{aa}}$ values for the aromatic residues Trp and Tyr, on the other hand, depend strongly on position. They are very unfavorable in the central 10-amino-acid zone, but become quite favorable toward the ends, consistent with the strong interfacial preference of aro-

matic amino acids. Interestingly, Phe does not show this effect. Its behavior is about the same as that of Leu. $\Delta G_{\text{app}}^{\text{aa}}$ values for charged residues, which can be placed in the middle of a TM segment in the presence of a sufficiently large number of Leu residues, show an even stronger dependence than Trp and Tyr. The positional penalty declines almost linearly as the residue is moved toward either end of the helix.

(B) TM helices with low hydrophobic moments (low amphiphilicity) are released into the bilayer interior from the translocon more readily than helices with high amphiphilicity.

(C) Surprisingly, the KvAP potassium channel voltage sensor (S4 helix) can be inserted across the ER membrane with good efficiency, despite the presence of four arginines. The strong positional dependence of $\Delta G_{\text{app}}^{\text{Arg}}$ makes this possible [106].

prevails despite great thermal motion. Understanding and describing the lipid bilayer and its interactions with proteins from this perspective is one of the important challenges ahead.

Acknowledgments

This work was supported by grants from the National Institute of General Medical Sciences (GM46823 and GM68002) to S.H.W., and the Swedish Cancer Foundation, the Swedish Research Council, and the Marianne and Marcus Wallenberg Foundation to G.v.H.

References

- 1 J.K. Lanyi, B. Schobert, *J. Mol. Biol.* **2003**, *328*, 439–450.
- 2 S.H. White, Hydrophathy plots and the prediction of membrane protein topology. In *Membrane Protein Structure: Experimental Approaches*, White, S.H. (ed.). New York: Oxford University Press, **1994**, pp. 97–124.
- 3 J.U. Bowie, *Protein Sci.* **1999**, *8*, 2711–2719.
- 4 R. Dutzler, E.B. Campbell, M. Cadene, B.T. Chait, R. MacKinnon, *Nature* **2002**, *415*, 287–294.
- 5 R.M. Stroud, L.J.W. Miercke, J. O’Connell, S. Khademi, J.K. Lee, J. Remis, W. Harries, Y. Robles, D. Akhavan, *Curr. Opin. Struct. Biol.* **2003**, *13*, 424–431.
- 6 Y.X. Jiang, A. Lee, J.Y. Chen, V. Ruta, M. Cadene, B.T. Chait, R. MacKinnon, *Nature* **2003**, *423*, 33–41.
- 7 B. Van den Berg, W.M. Clemons, Jr, I. Collinson, Y. Modis, E. Hartmann, S.C. Harrison, T.A. Rapoport, *Nature* **2004**, *427*, 36–44.
- 8 W.M. Clemons, Jr, J.-F. Ménétret, C.W. Akey, T.A. Rapoport, *Curr. Opin. Struct. Biol.* **2004**, *14*, 390–396.
- 9 S.H. White, G. von Heijne, *Curr. Opin. Struct. Biol.* **2004**, *14*, 397–404.
- 10 A.J.M. Driessen, E.H. Manting, C. van der Does, *Nat. Struct. Biol.* **2001**, *8*, 492–498.
- 11 R.E. Dalbey, G. von Heijne (eds), *Protein Targeting Transport and Translocation*. New York: Academic Press, **2002**.
- 12 S. Pfeffer, *Cell* **2003**, *112*, 507–517.
- 13 E. Bibi, *Trends Biochem. Sci.* **1998**, *23*, 51–55.
- 14 A.E. Johnson, M.A. van Waes, *Annu. Rev. Cell Dev. Biol.* **1999**, *15*, 799–842.
- 15 G. von Heijne, *Adv. Protein Chem.* **2003**, *63*, 1–18.
- 16 M.A. Lemmon, D.M. Engelman, *Q. Rev. Biophys.* **1994**, *27*, 157–218.
- 17 S.H. White, W.C. Wimley, *Annu. Rev. Biophys. Biomol. Struct.* **1999**, *28*, 319–365.
- 18 J.-L. Popot, D.M. Engelman, *Annu. Rev. Biochem.* **2000**, *69*, 881–922.
- 19 S.H. White, A.S. Ladokhin, S. Jaysinghe, K. Hristova, *J. Biol. Chem.* **2001**, *276*, 32395–32398.
- 20 S.H. White, *FEBS Lett.* **2003**, *555*, 116–121.
- 21 L.K. Tamm, H. Hong, Folding of membrane proteins. In *Protein Folding Handbook I*, Buchner, J., Kiefhaber, T. (eds). Weinheim: Wiley-VCH, **2004**, pp. 994–1027.
- 22 L.K. Tamm, A. Arora, J.H. Kleinschmidt, *J. Biol. Chem.* **2001**, *276*, 32399–32402.
- 23 T. Hessa, H. Kim, K. Bihlmaler, C. Lundin, J. Boekel, H. Andersson, I. Nilsson, S.H. White, G. von Heijne, *Nature* **2005**, *433*, 377–381.
- 24 J.H. Hurley, S. Misra, *Annu. Rev. Biophys. Biomol. Struct.* **2000**, *29*, 49–79.
- 25 Y. Liu, D.W. Bolen, *Biochemistry* **1995**, *34*, 12884–12891.
- 26 S. Tristram-Nagle, H.I. Petrache, J.F. Nagle, *Biophys. J.* **1998**, *75*, 917–925.
- 27 H.I. Petrache, S. Tristram-Nagle, J.F. Nagle, *Chem. Phys. Lipids* **1998**, *95*, 83–94.
- 28 J.F. Nagle, S. Tristram-Nagle, *Curr. Opin. Struct. Biol.* **2000**, *10*, 474–480.

- 29 J. F. Nagle, S. Tristram-Nagle, *Biochim. Biophys. Acta* **2001**, *1469*, 159–195.
- 30 S. H. White, M. C. Wiener, Determination of the structure of fluid lipid bilayer membranes. In *Permeability and Stability of Lipid Bilayers*, Disalvo, E. A., Simon, S. A. (eds). Boca Raton: CRC Press, **1995**, pp. 1–19.
- 31 S. H. White, M. C. Wiener, The liquid-crystallographic structure of fluid lipid bilayer membranes. In *Membrane Structure and Dynamics*, Merz, K. M., Roux, B. (eds). Boston: Birkhäuser, **1996**, pp. 127–144.
- 32 M. C. Wiener, S. H. White, *Biophys. J.* **1992**, *61*, 434–447.
- 33 S. H. White, W. C. Wimley, *Biochim. Biophys. Acta* **1998**, *1376*, 339–352.
- 34 A. S. Ladokhin, R. Legmann, R. J. Collier, S. H. White, *Biochemistry* **2004**, *43*, 7451–7458.
- 35 M. P. Rosconi, G. Zhao, E. London, *Biochemistry* **2004**, *43*, 9127–9139.
- 36 M. H. Gelb, W. H. Cho, D. C. Wilton, *Curr. Opin. Struct. Biol.* **1999**, *9*, 428–432.
- 37 J. G. Bollinger, K. Diraviyam, F. Ghomashchi, D. Murray, M. H. Gelb, *Biochemistry* **2004**, *43*, 13293–13304.
- 38 A. A. Frazier, M. A. Wisner, N. J. Malmberg, K. G. Victor, G. E. Fanucci, E. A. Nalefski, J. J. Falke, D. S. Cafiso, *Biochemistry* **2002**, *41*, 6282–6292.
- 39 K. Hristova, C. E. Dempsey, S. H. White, *Biophys. J.* **2001**, *80*, 801–811.
- 40 K. Hristova, W. C. Wimley, V. K. Mishra, G. M. Anantharamaiah, J. P. Segrest, S. H. White, *J. Mol. Biol.* **1999**, *290*, 99–117.
- 41 K. He, S. J. Ludtke, D. L. Worcester, H. W. Huang, *Biophys. J.* **1996**, *70*, 2659–2666.
- 42 L. Yang, T. M. Weiss, R. I. Lehrer, H. W. Huang, *Biophys. J.* **2000**, *79*, 2002–2009.
- 43 W. T. Heller, A. J. Waring, R. I. Lehrer, T. A. Harroun, T. M. Weiss, L. Yang, H. W. Huang, *Biochemistry* **2000**, *39*, 139–145.
- 44 J. P. Bradshaw, M. J. M. Darkes, T. A. Harroun, J. Katsaras, R. M. Epand, *Biochemistry* **2000**, *39*, 6581–6585.
- 45 T. M. Weiss, P. C. A. van der Wel, J. A. Killian, R. E. Koeppe, II, H. W. Huang, *Biophys. J.* **2003**, *84*, 379–385.
- 46 J. P. Bradshaw, S. M. A. Davies, T. Hauss, *Biophys. J.* **1998**, *75*, 889–895.
- 47 F.-Y. Chen, M.-T. Lee, H. W. Huang, *Biophys. J.* **2003**, *84*, 3751–3758.
- 48 R. W. Pastor, *Curr. Opin. Struct. Biol.* **1994**, *4*, 486–492.
- 49 D. P. Tieleman, S. J. Marrink, H. J. C. Berendsen, *Biochim. Biophys. Acta* **1997**, *1331*, 235–270.
- 50 L. R. Forrest, M. S. P. Sansom, *Curr. Opin. Struct. Biol.* **2000**, *10*, 174–181.
- 51 S. E. Feller, *Curr. Opin. Colloid Interface Sci.* **2000**, *5*, 217–223.
- 52 S. S. Deol, P. J. Bond, C. Domene, M. S. P. Sansom, *Biophys. J.* **2004**, *87*, 3737–3749.
- 53 S. E. Feller, K. Gawrisch, T. B. Woolf, *J. Am. Chem. Soc.* **2003**, *125*, 4434–4435.
- 54 D. P. Tieleman, B. Hess, M. S. P. Sansom, *Biophys. J.* **2002**, *83*, 2393–2407.
- 55 F. Q. Zhu, E. Tajkhorshid, K. Schulten, *Biophys. J.* **2004**, *86*, 50–57.
- 56 S. Bernèche, B. Roux, *Nature* **2001**, *414*, 73–77.
- 57 D. J. Tobias, Membrane simulations. In *Computational Biochemistry and Biophysics*, Becker, O. M., MacKerell, A. D., Jr, Roux, B., Watanabe, M. (eds). New York: Marcel Dekker, **2001**, pp. 465–496.
- 58 R. W. Benz, F. Castro-Román, D. J. Tobias, S. H. White, *Biophys. J.* **2005**, in press.
- 59 R. E. Jacobs, S. H. White, *Biochemistry* **1989**, *28*, 3421–3437.
- 60 J.-L. Popot, D. M. Engelman, *Biochemistry* **1990**, *29*, 4031–4037.
- 61 A. R. Curran, D. M. Engelman, *Curr. Opin. Struct. Biol.* **2003**, *13*, 412–417.
- 62 W. C. Wimley, S. H. White, *Nat. Struct. Biol.* **1996**, *3*, 842–848.
- 63 A. S. Ladokhin, S. H. White, *J. Mol. Biol.* **2001**, *309*, 543–552.
- 64 W. C. Wimley, K. Hristova, A. S. Ladokhin, L. Silvestro, P. H. Axelsen, S. H. White, *J. Mol. Biol.* **1998**, *277*, 1091–1110.
- 65 A. S. Ladokhin, S. H. White, *J. Mol. Biol.* **1999**, *285*, 1363–1369.
- 66 T. Wieprecht, M. Beyermann, J. Seelig, *Biochemistry* **1999**, *38*, 10377–10387.
- 67 Y. Li, X. Han, L. K. Tamm, *Biochemistry* **2003**, *42*, 7245–7251.

- 68 W. C. Wimley, S. H. White, *Biochemistry* **2000**, *39*, 4432–4442.
- 69 M. A. Roseman, *J. Mol. Biol.* **1988**, *201*, 621–625.
- 70 N. Ben-Tal, D. Sitkoff, I. A. Topol, A.-S. Yang, S. K. Burt, B. Honig, *J. Phys. Chem. B* **1997**, *101*, 450–457.
- 71 N. Ben-Tal, A. Ben-Shaul, A. Nicholls, B. Honig, *Biophys. J.* **1996**, *70*, 1803–1812.
- 72 S. Jayasinghe, K. Hristova, S. H. White, *J. Mol. Biol.* **2001**, *312*, 927–934.
- 73 J. P. Segrest, R. L. Jackson, V. T. Marchesi, R. B. Guyer, W. Terry, *Biochem. Biophys. Res. Commun.* **1972**, *49*, 964–969.
- 74 W. C. Wimley, T. P. Creamer, S. H. White, *Biochemistry* **1996**, *35*, 5109–5124.
- 75 S. Jayasinghe, K. Hristova, S. H. White, *Protein Sci.* **2001**, *10*, 455–458.
- 76 W. C. Wimley, K. Gawrisch, T. P. Creamer, S. H. White, *Proc. Natl Acad. Sci. USA* **1996**, *93*, 2985–2990.
- 77 M. Monné, M. Hermansson, G. von Heijne, *J. Mol. Biol.* **1999**, *288*, 141–145.
- 78 M. Monné, I. M. Nilsson, A. Elofsson, G. von Heijne, *J. Mol. Biol.* **1999**, *293*, 807–814.
- 79 I. M. Nilsson, A. E. Johnson, G. von Heijne, *J. Biol. Chem.* **2003**, *278*, 29389–29393.
- 80 K. A. Dill, *Biochemistry* **1990**, *29*, 7133–7155.
- 81 C. Tanford, *The Hydrophobic Effect: Formation of Micelles and Biological Membranes*. New York: Wiley, **1973**.
- 82 M. A. Lemmon, J. M. Flanagan, J. F. Hunt, B. D. Adair, B. J. Bormann, C. E. Dempsey, D. M. Engelman, *J. Biol. Chem.* **1992**, *267*, 7683–7689.
- 83 M. A. Lemmon, H. R. Treutlein, P. D. Adams, A. T. Brünger, D. M. Engelman, *Nat. Struct. Biol.* **1994**, *1*, 157–163.
- 84 K. R. MacKenzie, J. H. Prestegard, D. M. Engelman, *Science* **1997**, *276*, 131–133.
- 85 K. G. Fleming, A. L. Ackerman, D. M. Engelman, *J. Mol. Biol.* **1997**, *272*, 266–275.
- 86 K. R. MacKenzie, D. M. Engelman, *Proc. Natl Acad. Sci. USA* **1998**, *95*, 3583–3590.
- 87 J. U. Bowie, *J. Mol. Biol.* **1997**, *272*, 780–789.
- 88 D. Langosch, J. Heringa, *Proteins* **1998**, *31*, 150–159.
- 89 W. P. Russ, D. M. Engelman, *Proc. Natl Acad. Sci. USA* **1999**, *96*, 863–868.
- 90 W. P. Russ, D. M. Engelman, *J. Mol. Biol.* **2000**, *296*, 911–919.
- 91 A. Senes, M. Gerstein, D. M. Engelman, *J. Mol. Biol.* **2000**, *296*, 921–936.
- 92 F. X. Zhou, M. J. Cocco, W. P. Russ, A. T. Brünger, D. M. Engelman, *Nat. Struct. Biol.* **2000**, *7*, 154–160.
- 93 C. Choma, H. Gratkowski, J. D. Lear, W. F. DeGrado, *Nat. Struct. Biol.* **2000**, *7*, 161–166.
- 94 S. O. Smith, C. S. Smith, B. J. Bormann, *Nat. Struct. Biol.* **1996**, *3*, 252–258.
- 95 A. Kuhn, M. Spiess, Membrane protein insertion into bacterial membranes and the endoplasmic reticulum. In *Protein Targeting Transport and Translocation*, Dalbey, R. E., von Heijne, G. (eds). New York: Academic Press, **2002**, pp. 107–130.
- 96 V. Goder, M. Spiess, *FEBS Lett.* **2001**, *504*, 87–93.
- 97 R. Beckmann, C. M. T. Spahn, N. Eswar, J. Helmers, P. A. Penczek, A. Sali, J. Frank, G. Blobel, *Cell* **2001**, *107*, 361–372.
- 98 D. G. Morgan, J.-F. Ménétrete, A. Neuhof, T. A. Rapoport, C. W. Akey, *J. Mol. Biol.* **2002**, *324*, 871–886.
- 99 W. Mothes, S. U. Heinrich, R. Graf, I. M. Nilsson, G. von Heijne, J. Brunner, T. A. Rapoport, *Cell* **1997**, *89*, 523–533.
- 100 S. U. Heinrich, W. Mothes, J. Brunner, T. A. Rapoport, *Cell* **2000**, *102*, 233–244.
- 101 H. Chen, D. A. Kendall, *J. Biol. Chem.* **1995**, *270*, 14115–14122.
- 102 I. M. Nilsson, G. von Heijne, *J. Mol. Biol.* **1998**, *284*, 1185–1189.
- 103 K. A. Williams, C. M. Deber, *Biochemistry* **1991**, *30*, 8919–8923.
- 104 A. Sääf, E. Wallin, G. von Heijne, *Eur. J. Biochem.* **1998**, *251*, 821–829.
- 105 D. Eisenberg, R. M. Weiss, T. C. Terwilliger, *Proc. Natl Acad. Sci. USA* **1984**, *81*, 140–144.
- 106 T. Hessa, S. H. White, G. von Heijne, *Science* **2005**, *307*, 1427.

- 107 Y.X. Jiang, V. Ruta, J.Y. Chen, A. Lee, R. MacKinnon, *Nature* **2003**, 42–48.
- 108 M. Grabe, H. Lecar, Y.N. Jan, L.Y. Jan, *Proc. Natl Acad. Sci. USA* **2004**, *101*, 17640–17645.
- 109 A. Parsegian, *Nature* **1969**, *221*, 844–846.
- 110 K.J. Oh, L. Senzel, R.J. Collier, A. Finkelstein, *Proc. Natl Acad. Sci. USA* **1999**, *96*, 8467–8470.
- 111 R. Dutzler, E.B. Campbell, R. MacKinnon, *Science* **2003**, *300*, 108–112.
- 112 C.D. Snow, H. Nguyen, V.S. Pande, M. Gruebele, *Nature* **2002**, *420*, 102–106.
- 113 V. Goder, T. Junne, M. Spiess, *Mol. Biol. Cell* **2004**, *15*, 1470–1478.
- 114 D.J. Schnell, D.N. Hebert, *Cell* **2003**, *112*, 491–505.
- 115 W. Humphrey, W. Dalke, K. Schulten, *J. Mol. Graphics* **1996**, *14*, 33–38.
- 116 M.C. Wiener, S.H. White, *Biophys. J.* **1991**, *59*, 162–173.
- 117 S.H. White, K. Hristova, Peptides in lipid bilayers: determination of location by absolute-scale X-ray refinement. In *Lipid Bilayers. Structure and Interactions*, Katsaras, J., Gutberlet, T. (eds). Berlin: Springer, **2000**, pp. 189–206.
- 118 S.H. White, W.C. Wimley, *Curr. Opin. Struct. Biol.* **1994**, *4*, 79–86.
- 119 I.T. Arkin, K.R. MacKenzie, L. Fisher, S. Aimoto, D.M. Engelman, S.O. Smith, *Nat. Struct. Biol.* **1996**, *3*, 240–243.
- 120 T. Wieprecht, O. Apostolov, M. Beyermann, J. Seelig, *J. Mol. Biol.* **1999**, *294*, 785–794.

